HST/WFPC2 Observations of Warm Ultraluminous Infrared Galaxies[1]

Jason A. Surace, D. B. Sanders, William D. Vacca

University of Hawaii, Institute for Astronomy, 2680 Woodlawn Dr., Honolulu, HI, 96822

Electronic mail: jason, sanders, vacca@ifa.hawaii.edu

Sylvain Veilleux

University of Maryland, Department of Astronomy, College Park, MD 20742

Electronic mail: veilleux@astro.umd.edu

J. M. Mozzarella

Infrared Processing & Analysis Center, MS 100-22, California Institute of Technology, Jet Propulsion Laboratory, Pasadena, CA 91125

Electronic mail: mazz@ipac.caltech.edu

Received _____, accepted _____

*Based on observations with the NASA/ESA *HST*, obtained at the Space Telescope Science Institute, which is operated by the Association of Universities for Research in Astronomy, Inc., under NASA Contract NAS5-26555

1. Introduction

One of the most important results of the *Infrared Astronomical Satellite*[2] (*IRAS*) all-sky survey was the discovery of a significant population of galaxies that emit the bulk of their luminosity in the far-infrared (e.g. Soifer et al. 1984). Studies of the properties of these '(infrared" galaxies showed systematic trends coupled to the total far-infrared luminosity; more luminous systems were more likely to appear to be merger remnants or interacting pairs, and were more likely to possess AGN- like emission line features. A more complete review of the properties of luminous infrared galaxies can be found in Sanders & Mirabel (1996). Much recent attention has been focused on ultraluminous infrared galaxies (ULIGs), objects with infrared luminosities, L_{ir}[3], greater than $10^{12} L_{\odot}$, which corresponds to the bolometric luminosity of QSOS (i.e. M_B < –22.1: Schmidt & Green 1983). Multiwavelength observations of a complete sample of 10 ULIGs led Sanders et al. (1988a) to suggest that these objects might plausibly represent the initial dust- enshrouded stage in the evolution of optically selected QSOS, and that the majority, if not all QSOS may begin their lives in such an intense infrared phase.

An important subset of ULIGs are those objects with "warm" (f_{25}/f_{60} > 0.2) 4, mid-infrared colors. These warm objects, which represent ~ 20–25 % of the total population

---

[2]The Infrared Astronomical Satellite was developed and operated by the US National Aeronautics and Space Administration (NASA), the Netherlands Agency for Aerospace Programs (NIVR), and the UK Science and Engineering Research Council (SERC).

[3] $L_{ir} \equiv$ L(8 – 1000pm) is computed using the flux in all four *IRAS* bands according to the prescription given in Perault (1987); see also Sanders & Mirabel (1996). Throughout this paper we use H_o = 75 km $s^{-1} Mpc^{-1}$, q_o = 0.5 (unless otherwise noted).

[4]The quantities f_{12}, f_{25}, f_{60}, and f_{100} represent the *IRAS* flux densities in Jy at 12 μm, 25 μm, 60 μm, and 100pm respectively.

Cycles 3-5). The nine targets observed by us are listed in Table 1 along with the target coordinates, redshift, infrared luminosity, and the *HST* exposure times.

An initial description of the properties of the complete sample as determined from ground-based studies - including optical morphology, optical spectral type, and the radio-to-UV spectral energy distribution (SED) - was presented in Sanders et al. (1988 b). Three of the 12 warm ULIGs (I Zw I, Mrk 1014, and 3C273) were previously classified as optical QSOS , while the remainder are type 1 or 2 Seyferts. Six of the 12 objects have a dominant pointlike optical nucleus on the Palomar Sky Survey plates, similar in appearance to optically selected QSOs. Deep ground-based optical images show that three of the 12 have double nuclei while most of the remaining objects exhibit large-scale tidal features characteristic of advanced mergers. A more complete description of each the nine objects observed by us with *HST* is given in the Appendix. Ground-based images are also shown in Figure 1.

Since all of the warm ULIGs in our sample are at redshifts 0.05-0.15, the physical resolution achievable optically from the ground is only about 1–2 kpc, which is clearly insufficient to disentangle such structures as nuclear bars or rings that, for example, might be associated with a circumnuclear starburst, or to disentangle the relative contributions of such a starburst from any AGN component that might be present. The higher resolution of *HST* also permits much more accurate photometry, allowing for example, a more detailed examination of stellar populations. Finally, the low background in space, accompanied by the increase in point source detectability due to higher spatial resolution, enables us to search for very faint high spatial frequency structure.

4. Data Reduction

Dark subtraction, bias subtraction, and flat-fielding were carried out using the standard data reduction pipeline procedures at STScI. The spacecraft was commanded to keep the field in a fixed position and orientation throughout the observations, eliminating the need for later registration. This was confirmed by examining the location of the centroids of the nuclei, stars in the frame, and the extended structure. The image rotation introduced by the roll angle of the spacecraft was removed by rotating the image using linear interpolation according to the amount specified by STScI based on spacecraft telemetry. All photometric analysis was carried out on the unrotated images in order to avoid the small uncertainties introduced by the rotation process. Images were combined using the IRAF/STSDAS routine GCOMBINE which includes an algorithm for removal of cosmic rays from individual frames (effectively filling them in with good pixels from other frames). Saturated pixels in the bright nuclei were similarly replaced with data from the short exposures. Any remaining bad pixels (cosmic-ray hits, etc.) were identified by eye on the basis of their being radically inconsistent with the WFPC2 point-spread function (i.e. they were only a single pixel) and were filled in by linear interpolation between surrounding pixels. Since this was at most a few hundred pixels over the entire image, it is unlikely that many pixels in the sources themselves were lost.

Cosmic rays are particularly troublesome with the WFPC2 instrument. Due to the instrument's undersampling of the point spread function (PSF), it is difficult to differentiate single cosmic-ray hits from actual pointlike targets. Although the taking of multiple frames alleviates much of this problem, the high rate of cosmic-ray incidence can result in the same pixel being contaminated in multiple frames. This was checked by creating frames which were constructed of only the lowest value pixels in an image stack; this procedure should reject all cosmic rays except those unlikely few which contaminate every frame.

for reddening. The most distant target is at redshift z = 0.16 and the median redshift for the sample is only z = 0.09; thus K-corrections are likely to be quite small. Based on stellar synthesis models which are believed to be representative of some of these features (see below), theoretical K-corrections were computed and found to indeed be generally very small, typically Am = 0.1 in the B and I filters at z = 0.16 for systems 10^7– 10^8 yrs old, with extremes of Δm = 0.4 for extremely blue or red systems. K-corrections are not believed to affect derived colors by more than $\Delta(B-I) = 0.4$. Finally, since no actual observational spectral energy distributions (SEDs) exist for the features in these objects, it was felt that the uncertainties in assigning K-corrections probably outweighed any real benefit.

More importantly, no reddening corrections have been made to any magnitudes reported in this paper. The reddening in some regions of these galaxies may be quite large; Kim (1995) reports typical extinctions based on optical spectroscopy of 2-6 Av for the central (2") regions of these systems, and of 4.5 Av for Seyfert-like ULIGs in general. The effects of reddening are more thoroughly discussed in §6.2.

5. Results

5.1. Large-Scale Morphology and Colors

Figure 2 displays the large scale structure seen in the PC2 observations of each of the observed ULIGs. Eight of the nine ULIGs (except IRAS 01003–2238) show clear signs of recent merger activity in the form of tidal tails and loops. Additionally, IRAS 08572+3915, Pks 1345+12, and Mrk 463 have clear double nuclei. Further details can be seen in the truecolor display of Plate 1 which shows the full field-of-view for each of the 9 objects. Figures 3 & 4 show close-ups of the individual nuclear regions in each ULIG (small boxes

IRAS 01003–2238, Mrk 1014, and Pks 1345+12 have a reasonably simple color structure, perhaps indicating the presence of a uniform (if any) dust screen. The other six galaxies have a variety of different features. This varies from organized structures like the face-on spiral pattern of Mrk 231 and the dust lane which seems to bisect IRAS 05189–2524, to the rather chaotic pattern seen in IRAS 12071 –0444 and the northwest nucleus of IRAS 08572+3915. Typical colors for spiral galaxies are $B-I=$ 1.8 (Lu et al. 1993). As expected, in most cases the detectable background light in these galaxies is similar to this value. It is also apparent from the colormaps that many of the ULIGs (notably Mrk 231, Mrk 463, and IRAS 15206+3342) show evidence of large numbers of blue (B-$I \leq$ 1.0) pointlike features.

5.2. Knots

We have identified in each of the galaxies bright compact regions which are usually bluer than the underlying galaxy and which appear similar to the bright blue knots found in other interacting galaxies (e.g. NGC 4038/9 - Whitmore & Schweizer 1995). While three of the observed galaxies (Mrk 1014, IRAS 05189–2524, and Pks 1345+12) seem to have very few of these "knots", the remaining six have as many as 30 each (in the cases of Mrk 231 and Mrk 463). The mean number of knots per galaxy is 13. Their locations are illustrated in Figure 6 and given in Table 2. For those systems with many knots, approximately half lie within 2 kpc of what appear to be nuclei (see § 5.3) while the remainder are spread along what appear to be inner tidal features (e.g. IRAS 08573+3915 and Mrk 463). The knots often appear to be arranged in linear structures or "strings" one or two knot widths wide and 4–5 knots long (the best examples can be found in IRAS 01003–2238, IRAS 12071–0444, Mrk 231, and IRAS 15206–3342).

The apparent magnitudes were measured for each of the identified knots. Initially,

and decreased to about 0.05 magnitudes at 23 magnitudes and brighter. This is similar to the expected result based on the image noise statistics. Since most of the knots fall in the magnitude range from 22 to 26 (the 3σ limiting magnitude based on image noise statistics is generally between 26–27), a reliable uncertainty from measurement is about 0.15. Systematic due to calibration problems (see §4) and aperture effects contribute another 0.1 magnitudes. Since the systematic probably affect both filters nearly equally, the associated error in color is only a function of measurement uncertainties, and is around 0.2-0.3.

5.3. Putative Nuclei

Within the general population of knots that were identified for each object there were one or two knots which we believe plausibly represent putative nuclei. Not only are these the brightest knots at B, but they are also usually the most pointlike, and more importantly they are spatially coincident with dominant K-band peaks in high-resolution K-band images that have recently been obtained with the University of Hawaii 2.2m telescope (Surace et al. 1997). The properties of these putative nuclei can be found in Table 2, including the implausibly large masses that would be implied if these if these objects were interpreted as starbursts (see §6.2 below).

5.4. *IRAS* 07598+6508, I Zw 1, 3C273

HST images of the three objects in our complete sample of 12 warm ULIGs that were not observed in our Cycle 5 GO program have either recently been published or can be found in the *HST* archive. These three objects have the smallest far-infrared/submillimeter excess of the 12 warm ULIGs and all of them exhibit Seyfert 1 optical spectra, Of the three,

make the identification of any circumnuclear knots that might be present extremely difficult.

In summary, *IRAS*07598+6508 and I Zw 1 have several properties in common with the other nine sources observed by us, including luminous knots and arm-like circumnuclear features, as well as luminous hosts. 3C273, other than its jet-like feature and the presence of a luminous host, has yet to reveal knots and other large scale features that are seen in the other sources in our complete sample of warm ULIGs. However, given that these three objects were not observed by us, they will not be included further in the discussion of the data obtained for this paper.

6. Discussion

6.1. Large-scale features

Of the 9 warm ULIG observed by us with *HST*, eight are unmistakably advanced merger systems. This is perhaps expected since several recent studies have shown that >95 % of ULIGs are strongly interacting/merger systems (Sanders et al. 1988a, Melnick & Mirabel 1990, Kim 1995, Murphy et al. 1996, Clements et al. 1996). More interesting perhaps, (and indeed what our *HST* observations were designed to show), is the mean separation of the nuclei of the parent disks. Although our statistics are obviously limited by the small sample size, we find that the warm ULIG double nuclei fraction is considerably lower than that of "cold" ULIGS. As will be shown later, following our discussion of the knots observed in each object, only 4 of the nine observed warm galaxies have obvious double nuclei (44%), as opposed to $\gtrsim$ 60% found by Murphy (1995) for his ground-based images of cold ULIGs. Three of the four double-nucleus warm ULIGs were already known to be double from lower-resolution ground-based observations. What the enhanced resolution of *HST* has primarily revealed is that what were previously thought to be possible doubles (e.g.

are based on solar metallicity; no attempt has been made to explore metallicity effects as they are most likely unimportant compared to other uncertainties. A Salpeter IMF and a stellar mass distribution from 0.1 to 125 $M_{\odot}$ is assumed, although the actual mass distribution has little effect after an age of a few Myrs. This model is probably applicable to the majority of starburst regions (Leitherer 1996). The BC93 models were used to construct color-magnitude, M'_B vs. $(B-I)$, evolutionary tracks as a function of time for an instantaneous starburst of different total masses. These tracks, shown in Figure 7, illustrate that the knot age is a nearly monotonically increasing function of $B-I$ color, although there is a degeneracy in $B-I$ colors from approximately 107 to 108 yrs during which the model remains at essentially the same $B-I$ color ($= 0.7$). Perhaps not unsurprisingly, the mean knot color is very close to this value (Figure 8). Since the constraints on the absolute knot luminosity are relatively weak, it is not easy to estimate the knot fading and hence help determine the age from M'_B. Our knot ages are thus determined entirely from the $B-I$ color.

Knot masses are similarly derived from the BC93 models. The models for a 1 $M_{\odot}$ stellar ensemble were scaled to the observed absolute magnitude to derive a mass. In Figure 7 the evolutionary tracks illustrated are for knots of a given, fixed cluster mass.

Also shown in Figure 7 are the effects of 1 visual magnitude of reddening (Sapar & Kuusik 1978). There are rough estimates of the reddening in these galaxies. Kim (1995) examined optical spectra of 5 of the nine galaxies in our sample and concluded that the reddening varied typically from 2 Av (IRAS 15206+3342) to 6 Av (IRAS 08572+3915). Unfortunately, the slit size and extraction apertures of these spectra are so large that they are averaged over the entire central (≈ 2“) regions of the galaxies. The extremely complex morphology seen in the *HST* images suggests that the actual extinction is likely to be patchy in many of these systems. Additionally, an examination of the *HST* data in the apertures used for these spectra shows that the knots typically account for 10–4070 of the wide-band optical emission; they do not dominate it, and hence the reddening indicated by

(Figure 7). Furthermore, while in almost all 2-color diagrams that use B and longer wavelengths, the evolutionary tracks run parallel to the reddening vector while the (U-B) vs (B–I) track is nearly perpendicular to the reddening vector during this criticalperiod. Observations at U or shorter wavelengths will therefore remove both the time degeneracy and much of the reddening problem. Alternately, extremely high spatial resolution optical spectra would allow a direct determination of the reddening of each knot.

Since we expect the properties of the knots to be connected to the galaxy merger system as a whole, we discuss below the mean properties of the knots on a *per galaxy basis.* Following Whitmore & Schweizer (1995), if it is assumed that the spread in knot colors is due equally to the effects of reddening and intrinsic color due to age, then the mean reddening is $\sim$ 25 % of the spread in knot colors. The estimated mean reddening then varies from Av = *0.41* in IRAS 15206+3342 to Av = 0.08 in Mrk 1014. Applying no reddening correction, the knot colors imply ages varying from a mean of 7 Myr in Mrk 463 and IRAS 01003-2238 (corresponding to < $B-I$ >= 0.4) to 1.4 Gyr in IRAS 12071–0444 (corresponding to < $B-I$ >= 1.63). These represent upper limits to the mean knot ages in each galaxy. Applying the mean reddening correction shortens these ages to 6 and 370 Myr, respectively. The 6 remaining galaxies have upper limits to their mean knot ages of $\sim$ 6 x 10^8 yr (with no reddening correction). Note that if a reddening correction is applied to these 6 apparently older systems, then their ages may drop to as little as 0.6x 10^8 yr due to the degeneracy in B–I colors from 10^7 to 10^8 yr. Due to the uncertainties involved, no further corrections will be made for reddening. The mean age for *all* knots in all warm ULIGs is 5.7x 10^8 yr, while the median age is 0.1-2.5x 10^8 (the range being due to the color-age degeneracy). This latter figure is dominated by the large numbers of blue knots in Mrk463 and IRAS 01003-2238.

The five galaxies IRAS 01003–2238, IRAS 08572+3915, Mrk 231, Mrk 463, and IRAS 15206+3342 each contain at least a few knots whose ages cannot exceed 10 Myr.

extreme ages ($> 10^9$ yrs) or reddening are too faint at B to still be detected. However, it is the case that in the systems with many knots *there are no young, blue knots with estimated masses as large as the older, redder knots.* The above discussion of the correlation between color and radial distribution also extends to the knot masses: the most massive knots appear preferentially distributed closer to the galaxy nuclei.

6.3. **Knot Sizes**

In almost every case, the knots appear to be resolved in comparison both to the observed PSF and the TIM models. Knot radii were characterized by directly fitting the knots with radial Gaussian distributions and using the derived FWHM in order to estimate the width of the underlying distribution. This ha-s been done by several workers (Whitmore & Schweizer 1995, Meurer et al. 1995) and is probably a measure of the effective core radius, although others have argued that Hubble profiles with characteristic core and half-light radii may be more appropriate for knot measurements (Holtzman et al. 1996). Given that only rarely do the data have sufficient signal-to-noise to detect the low, broad wings of the Hubble profile, and that radial Gaussians seem to provide very good fits to the detected knot profiles, the use of Gaussians seems well-motivated from the standpoint of providing a useful number from the actual data, as opposed to having some more meaningful physical significance. In particular, it is useful for directly providing a size measurement, whereas the actual form of the fitting function primarily has significance in discussing the total luminosity of the knot. Note that the process of radial averaging and model-fitting effectively oversamples the data, so that it is possible to extract size information on spatial scales smaller than the Nyquist sampling one would achieve by merely fitting l-d cross-sections.

The actual measurements were performed by fitting radial Gaussians to the data

have an average R_{eff} of 65 pc, with the very largest being nearly 250 pc in radius. This is 2–3 times larger than the largest knots found in other systems, and many times larger than the mean knot radii: 18 pc in NGC 4038/9 (Whitmore & Schweizer 1995) and ≈ 10 pc in 9 starburst galaxies (Meurer et al. 1995). Schweizer derives a median upper limit of 5 pc for the clusters/knots in NGC 3921 (Schweizer et al. 1996) and Holtzman et al. (1996) finds typically 2–10 pc. Our largest knots are nearly 50 times larger than these and the 1.5–5 pc half-light radii of globular clusters (van den Bergh et al. 1991).

6.4. **Luminosity Function of Knots**

Figure 9 presents the luminosity functions of the knots in Mrk 231 and Mrk 463, the two systems with the largest number of knots. These functions appear similar to the bright tail of the cluster/knot luminosity functions found in more nearby interacting galaxies such as NGC 4038/9 and NGC 7552. The data were binned into 0.5 mag bins, which are sufficiently large that photometric uncertainties should have little effect on the form of the distribution. Additionally, the putative "nuclei" have not been included, since they are believed to be of non-stellar origin (see §6.5). A lower magnitude limit cutoff of M'_B = — 12.5 was chosen to ensure completeness in both systems. There is no direct evidence of a turnover in the knot luminosity function. This is not surprising: if we assume an age of 600 Myr for most of the knots, and a peak in the current galactic globular cluster distribution near $M_B \approx -8$, then the peak would occur in our (younger cluster) data near M_B = – 12, which is just fainter than our completeness limit. This makes the assumption that all the clusters are the same age; Meurer (1995b) argues that the luminosity function of burst-model clusters with continuous cluster formation more closely resembles the power-law observed by Whitmore & Schweizer (1995).

A power-law fit of the form

A more likely explanation is that the knots are associations of many of the clusters seen in nearer systems. Meurer (1995b) notes that the typical intercluster separation in some starburst regions may be $\leq$ 18 pc, which is too small to resolve in our observations. We note that the seeing-limited resolution of NGC 4038/9 from the ground ($1'' = 90$ pc for H_o = *75 km* s-l) is similar to the diffraction-limited resolution of the warm ULIGs that can be achieved with *HST* ($\approx$ *90* pc FWHM for IRAS15206+3342). Ground-based images of the central regions of NGC 4038/9 at B show a loop-like structure with bright embedded knots (Rubin et al. 1970). These knots (excluding the regions of the galaxy nuclei) have mean radii of $\approx$ 75 pc (derived from the 45 pc HWHM spatial resolution ground-based data using the methods described above) , varying from nearly unresolved to as large as 150 pc. This is very similar to the range seen in the warm ULIGs. Whitmore & Schweizer (1995) has determined that each of these knots in NGC 4038/9 is actually composed of many smaller clusters. The mean number of clusters per knot is 13, and correspondingly the knot as a whole is on average 2.8 mag brighter than the individual clusters. Assuming that the clusters associate in knots in an essentially random way, then shifting the NGC 4038/9 luminosity function by this amount results in the brightest knots being equivalent to $M_B \approx -18.5$. This is only a magnitude difference from the brightest of the knots seen in the warm ULIGs. The derived masses of the warm ULIGs are still somewhat too large. While the lowest mass knots in the ULIGs can be explained as aggregates of tens of typical clusters with spatial distributions of the kind seen in NGC 4038/9, the most massive ULIG knots like those in IRAS 15206+3342, approach $10^9 M_\odot$. This would require some 10^4 globular clusters or 50 of the most massive clusters observed by Whitmore & Schweizer (1995). This could be explained either by a very large reddening correction which would reduce the knot mass estimate by a factor of 15, by knots with larger total numbers of clusters due to a higher density than those seen in galaxies like NGC 4038/9, or by a preferential spatial distribution wherein extremely massive clusters tend to form together. The smaller luminosity function

luminosity. Only in the case of IRAS 15206+3342 would it be possible to approach within a factor of 10 the necessary luminosity.

Based on radio and far-infrared data, Condon et al. (1991) concluded that ULIGs contained ultraluminous starbursts in an environment so dense as to be optically thick even at 25 μm. A deeply embedded ultraluminous starburst composed of the optically observed star-forming knots would have to be at least 600-1200 pc in diameter. This is sufficiently large that it should be detectable in our images and color maps as a large region with a considerable color gradient or no detectable optical luminosity at all, although it might be possible to mask the presence of such a region with a peculiar overlying stellar distribution at lower optical depth. That such a large region is not observed in our data suggests that an ultraluminous starburst must be far more compact than the observed starburst knots. This is not surprising, considering that Condon et al. (1991) finds that ULIGs with $L_{\rm fir} > 10^{12}$ LO have radio emission typically dominated by compact radio sources. The three targets in the warm sample which he specifically examined have characteristic radio core sizes ranging from 0.1 to 80 pc in radius; additionally Mrk 1014 (Kellerman et al. 1994), Pks 1345+12 (Shaw et al. 1992) and Mrk 463 (Mozzarella et al. 1991) are also known to have compact cores. Based on the radio/far-infrared correlation it is argued that the starburst energy source is of a similar size. The minimum blackbody radii Condon derived from the far-infrared luminosities, which presumably are representative of the size of the enshrouding dust, are 0.15″= 150 pc for IRAS 05189–2524, 0.09″= 85 pc for IRAS 08572+3915, and 0.25”= 200 pc for Mrk 231. A single observed optical knot is similar to or larger than the expected size of the starburst region, and is nearly one- tenth as large as the volume of the dust shroud. Although such an obscured region containing very extreme star-formation is not clearly seen, it’s detection is complicated by the uncertainties in coordinate precession and in the relationship between the radio and optical coordinate systems. These uncertainties prevent the registration of the radio and optical images with

is similar to the reddening derived by assuming a reddened QSO nucleus (A_v = 3.5). The nuclei of Mrk 463, IRAS 12071–0444, IRAS 05189–2524, and IRAS 08572+3915 all show clear signs of complex extinction and scattering. Since the nuclei were defined to be a single component at *B*, any true nucleus affected by variable extinction and scattering would both fainter and bluer than it would if the extinction were uniform. This would move it to the lower left of the color-magnitude diagram, in the manner seen. lRAS 01003–2238 cannot be easily explained in this scenario, as it has a nearly stellar radial profile, yet falls considerably short of QSO-like luminosity.

We also note that the masses derived for the nuclei, under the assumption that they are a starburst of the sort modeled for the blue knots, are typically > 1010 $M_\odot$. This seems unreasonably large in light of the measured radii. In the case of Mrk 231 and Mrk 1014, this would result in average stellar densities of nearly 10^7 and 2 x $10^5 M_\odot pc^{-3}$, respectively. Similarly, IRAS 01003–2238, IRAS 05189–2524, and Pks 1345+12 all have derived stellar densities > $10^5 M_\odot pc^{-3}$. Elliptical galaxy cores typically have masses as high as $10^{10} M_\odot$, but they also have much smaller densities of $\approx 10^2 - 10^3 M_\odot pc^{-3}$. Similarly, although nuclear star clusters in galaxy cores may have very high densities (> $10^5 M_\odot pc^{-3}$), they have smaller masses ranging from $10^6 - 10^8 M_\odot$ (Lauer 1989). The remainder of the warm ULIG nuclei would require stellar densities of $10^3 M_\odot pc^{-3}$ and higher, which makes them denser than all but 7 of the knots and at the high end of elliptical core densities. The only exception is the eastern nucleus of IRAS 08572+3915, whose luminosity and color are consistent with a typical galaxy core, which it strongly resembles (see Appendix A).

Until high spatial resolution spectra are obtained, it will not be possible to determine whether the observed optical Seyfert activity is related to the putative nuclei that have been identified here. An interesting prediction of Condon et al. (1991) is that the observed broad optical emission line regions are a result of starburst/superwind activity and must be extended on size scales larger than the minimum far-infrared size ($\geq$ 0.25 pc). This

equal (e.g. Sanders & Mirabel 1996). Additional *HST* data, in particular spectroscopy of the emission knots discovered in both samples, may provide sufficient evidence to show whether or not the features observed in QSO hosts are indeed aged versions of those observed in the warm ULIGs.

7. Conclusions

From our new *HST* WFPC2 images of a nearly complete sample of warm ULIGs we draw the following conclusions:

1. Eight of the nine objects imaged show evidence that they are advanced merger systems. Three have clearly identified double nuclei, while an additional five objects show circumnuclear features that connect to larger scale tidal tails, fans and/or bridges that were previously identified in lower resolution ground-based images.

2. A population of compact, blue star-forming knots has been discovered in all of the warm ULIGs. These knots appear similar in radius and luminosity to the most luminous knots found in ground-based images of nearby merger LIGs such as NGC 4038/9 and Mrk 171. *HST* imaging shows that the luminous knots in these nearby systems break up into groups of several massive star-clusters that are assumed to be proto globular clusters. However, the warm ULIGs are too distant to be similarly resolved with *HST*.

3. The masses of the star-forming knots in the warm ULIGs are estimated to be in the range 10^5 — $10^9 M_\odot$. There is some evidence that the warm ULIGs have an overabundance of luminous (massive) knots compared to other nearby, less luminous merger systems. Their (extinction uncorrected) colors yield a median upper age for the starburst knots in a given system of $\sim 3 \times 10^8$ yrs. Regardless of reddening effects, several of the systems have knots which must be very young ($\approx 0.5 - 1 \times 10^7$ yrs). These young, blue knots are often found at

number HF- 1039. O1-92A awarded by the Space Telescope Science Institute which is operated by the AURA, Inc. for NASA under contract No. NAS5-26555. This work has made use of the NASA/IPAC Extragalactic Database (NED) which is operated by the Jet Propulsion Laboratory, California Institute of Technology, under contract with the National Aeronautics and Space Administration, and the Digitized Sky Survey (DSS), which was produced at the Space Telescope Science Institute under U.S. Government grant NAGW-2166. The DSS was produced using photographic data obtained with the Oschin Schmidt Telescope on Palomar Mountain, operated by the California Institute of Technology, and the UK Schmidt Telescope, which was operated by the Royal Observatory Edinburgh and the Anglo-Australian Observatory.

complete loop. There is no obvious connecting feature in the *HST* images which would connect the inner disk structure to the counter tidal tail previously identified by Sanders et al. (1988a) which extends to the South from the western edge of the disk.

IRAS 08572+3915: The new *HST* images clearly show the interaction of two spiral galaxies which have not yet merged. The eastern nucleus is morphologically similar to a spiral bulge from which a tidal tail 30 kpc in length emerges to the East and then wraps entirely around the system to the NW. Another tidal tail at least 15 kpc in length emerges from the western nucleus and extends directly north. A bridge of material is seen connecting the two nuclei. Unlike the nondescript eastern nucleus for which we find no published reference as to spectral type, the LINER western nucleus (Veilleux et al. 1995) is morphologically complex, with several bright blue knots as well as highly reddened regions. This disparity in optical appearance is not surprising and probably reflects very real differences in the environments of these two nuclei. This is supported by studies at 3.4μm (Zhou *et al.* 1993), 10pm (Sanders et al. 1988 b), and 1.66 Ghz (Sopp & Alexander 1991) which indicate that almost most of the bolometric luminosity of this object originates in the northwest nucleus.

IRAS 12071– **0444:** Sanders et al. (1988b) classify this galaxy on the basis of optical spectra as a Seyfert 2. In addition Veilleux, Sanders & Kim (1997) find strong evidence for a 'buried QSO' on the basis of detection of [Si VI] emission in the near infrared. The *HST* images show two tidal tails extending to the North and South. The southern tail loops back around to the northeast (although it is difficult to see in Figure 2) and appears to almost return to the nucleus, a total distance of 60 kpc; our *HST* images are not deep enough to tell if it reconnects. The inner 5 kpc region has a high surface brightness and is chaotic in appearance. A central, highly reddened compact source dominates this region. A string of blue knots 2.5 kpc in length runs to the West of the central source.

structures, and optical/near-infrared colors which have been interpreted by Mozzarella et al. (1991) as representative of a dusty QSO. An optical "jet" seen by Uomoto et al. (1993) resembles in our data an "X''- shaped structure dominated by a central peak. Tremonti et al. (1996) report that the bright object to its north is highly polarized and reflects a hidden Seyfert 1 nucleus lying in this "X"-structure. This is confirmed by high resolution near- infrared observations (Surace et al. 1997) which indicate that the near-infrared luminosity is centered on the "X". The entire eastern nucleus lies on a plateau of extended emission in which there are several bright knots. The western nucleus is optically classified as a Seyfert 2. There seem to be two principal components to the western nucleus: a dominant source which is distinctly elongated in the E-W direction, and a more compact, very blue source 1" to its West. Also in this region are two arcs of star-forming knots to the North and South of the two dominant components of the western nucleus. Both of these arcs form a sharp edge to a fan of emission centered on the dominant nuclear components.

IRAS 15206+3342: Sanders (1988b) classify this galaxy as a Seyfert 2 on the basis of optical spectra. The inner few kiloparsecs are characterized by many chains of knots, some of which are extremely luminous. Several of the knots have luminosities and colors compatible with being extremely massive starbursts, but there are two which make good candidates for being nuclei. Additional spectroscopic observations will be needed to identify unambiguously the source of Seyfert activity.

Leitherer, C. 1996, in From Stars to Galaxies, eds. C. Leitherer, U. Fritze-vonAlvensleben, J. Huchra (San Francisco: ASP), 373

Low, F. J., Huchra, J. P., Kleinmann, S. G., & Cutri, R. M. 1988, ApJ, 287, 95

Lu, N. Y., Hoffman, G. L., Groff, T., Roos, T., & Lamphier, C. 1993, ApJS, 88, 383

Mozzarella, J., Gaume, R., Soifer, B. T., Graham, J. R., Neugebauer, G., & Matthews, K. 1991, AJ, 102, 1241

Melnick, J., & Mirabel, I.F. 1990, å, 231, L9

Meurer, G., Heckman, T., Leitherer, C., Kinney, A., Robert, C., & Garnett, D. 1995, ApJ, 110, 2665

Meurer, G. 1995b Nature, 375, 742

Miller, J. S., & Goodrich, R.W. 1990, ApJ, 355, 456

Murphy, T., Armus, L., Matthews, K., Soifer, B. T., Mozzarella, J. M., Shupe, D. L., Strauss, M. A., & Neugebauer, G. 1996, AJ, 111, 1025

Peebles, J. Principles of Physical Cosmology, 1993 (Princeton: Princeton Univ. Press)

Perault, M. 1987, Ph.D. Thesis, University of Paris

Rubin, V., Ford, W., & D'Odorico, S. 1970, ApJ, 160, 801

Sanders, D. B., Scoville, N. Z., & Soifer, B. T. 1988, ApJ, 335, 1

Sanders, D. B., &Mirabel, I.F. 1996, ARA&A, 34, 749

Sanders, D. B., Soifer, B. T., Elias, J. H., Madore, B. F., Matthews, K., Neugebauer, G., & Scoville, N.Z. 1988a, ApJ, 325, 74

Sanders, D. B., Soifer, B. T., Elias, J. H., Neugebauer, G., & Matthews, K. 1988b, ApJ, 328, 35

Sapar, A., & Kuusik, I. 1978, Publ. Tartu. Astrophys. Ohs., 46, 71

Fig. 1.— The PC2 field-of-view (36″x 36”) superimposedon contour maps of the ground-based Gunn-r images of the nine warm ULIGs. The ground-based data are from Sanders et al. (1988 b). The galaxies are ordered by increasing R. A., from left to right, top to bottom: (1) IRAS 01003–2238, (2) Mrk 1014, (3) IRAS 05189–2524, (4) IRAS 08572+3915, (5) IRAS 12071-0444, (6) Mrk 231, (7) Pks 1345+12, (8) Mrk 463, and (9) IRAS 15206+3342. All images are displayed with North at the top and East to the left.

Fig. 2.— Large-scale structure of the nine warm ULIGs observed with the PC2 in *I*-band (F814W). In order to emphasize both faint and bright features, all images are block-averaged (3x3) and displayed with a non-linear stretch. Major ticks are 10”, except for IRASO1OO3–2238 and IRAS15206+3342 where each major tick is 5“. The scale bar represents 10 kpc. The white boxes indicate the individual nuclear regions that will be displayed in Figures 3-5.

Plate 1. — “Truecolor” images of the nine warm ULIGs. Order isthe same as in Figure 1: (1) IRASO1OO3–2238, (2) Mrk 1014, (3) IRAS 05189–2524, (4) IRAS08572+3915, (5) IRAS 12071–0444, (6) Mrk 231, (7) Pks 1345+12, (8) Mrk 463, and (9) IRAS 15206+3342. For these images, we have linearly interpolated the galaxy SED and then presented it as a color image. The result should be similar to the actual color, as *I* is mapped to red, and *B* to blue. Both color and luminosity information are presented simultaneously. Note that the colors are *not absolute*, i.e. the color balance changes from image to image depending on the S/N in the different observations.

Fig. 3.–- Close-up view of the nuclear regions of the warm ULIGs at *B*-band (F439W). The double nuclei in IRAS 08572+3915, Pks 1345+12, and Mrk 463 are displayed in separate panels labeled E (East) and W (West). The field of view represented by each of the 12 panels for the nine warm ULIGs is identical to the overlay boxes displayed in Figure 2. The major ticks are in arcseconds, and the scale bar represents 1 kpc.

of the warm ULIGs. For comparison with the remaining knots the shaded region indicates the locus of points for the data used in Figure 7. Extinction (A_V = 1) is indicated by the vector at upper right. Mrk 1014, a PG QSO, is typical of the colors found in optically selected QSOs. The nuclei for the remaining warm ULIGs in our sample fall roughly along what can be described as a QSO reddening line.

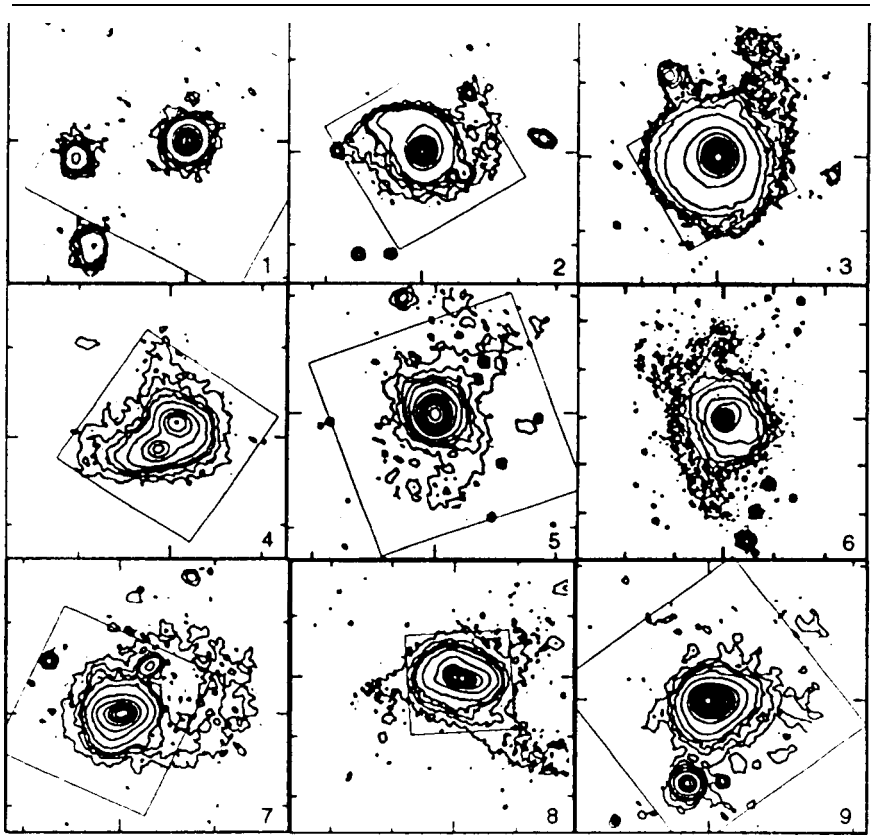

Fig. 1.-

Fig. 3. -

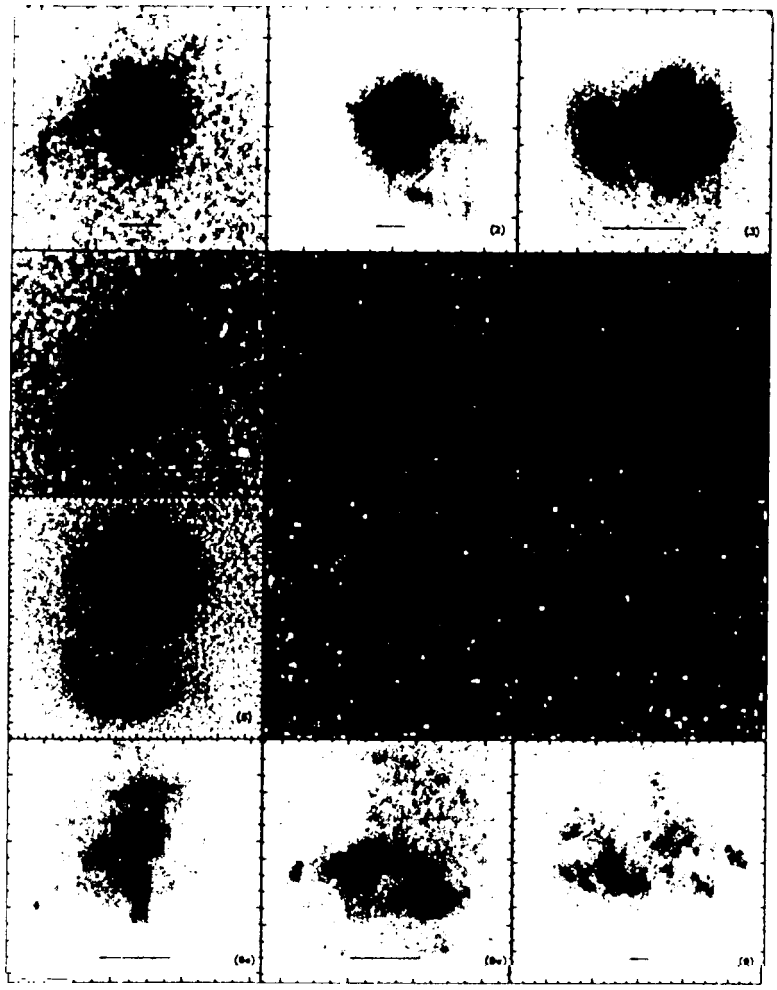

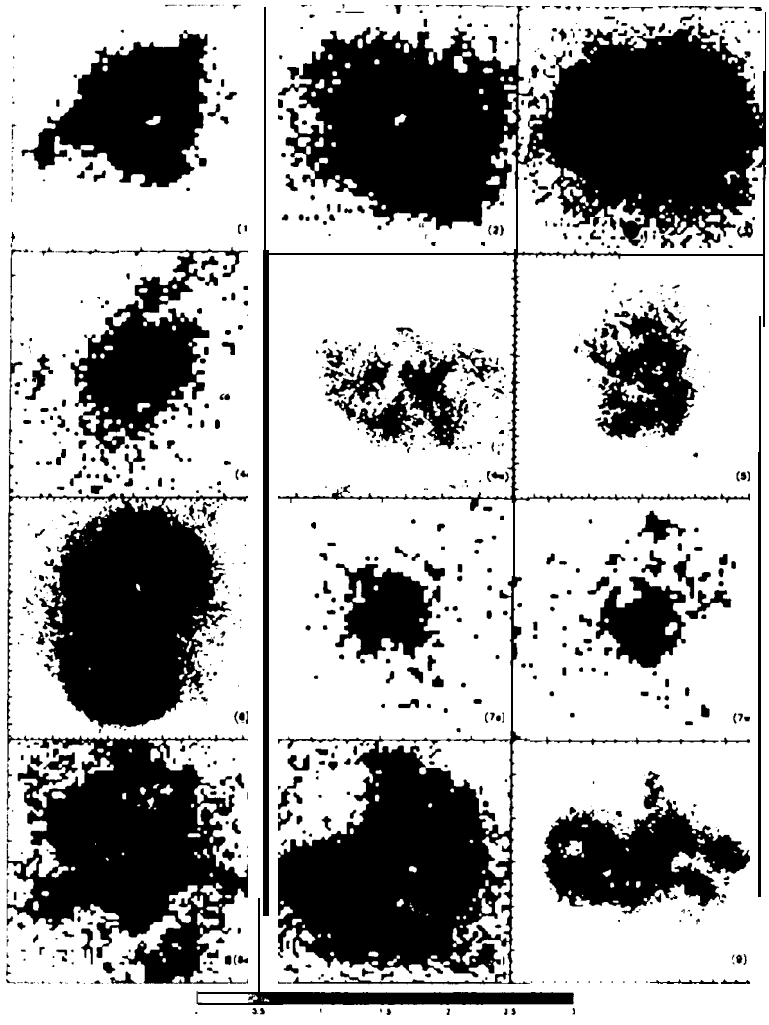

Fig. 5.—

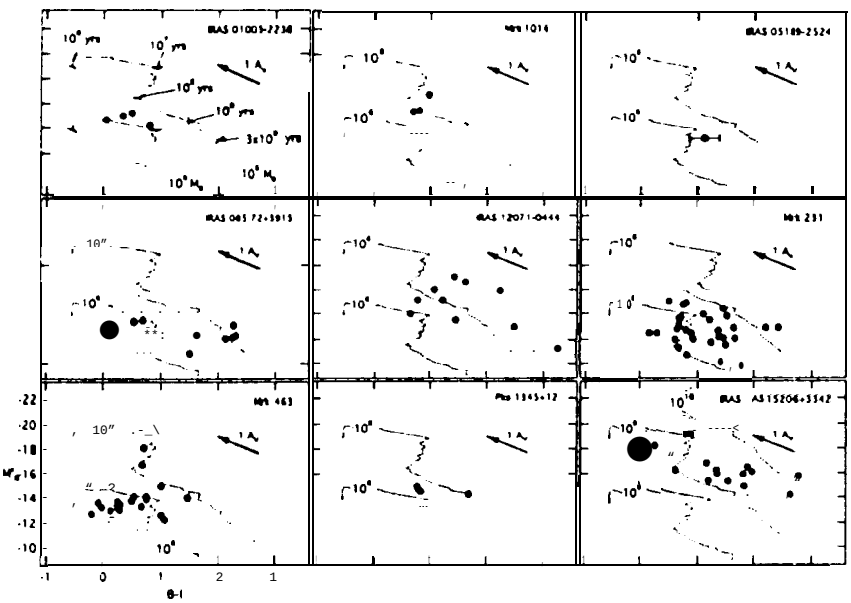
IRAS 01003-2238
Mrk 1014
IRAS 05189-2524
IRAS 08572+3915
IRAS 12071-0444
Mrk 231
Mrk 463
Pks 1345+12
IRAS F15206+3342
1 A_V
10^8 yrs
3x10^8 yrs
10^9 M_⊙
10"
M_V
B-I

Fig. 7.—

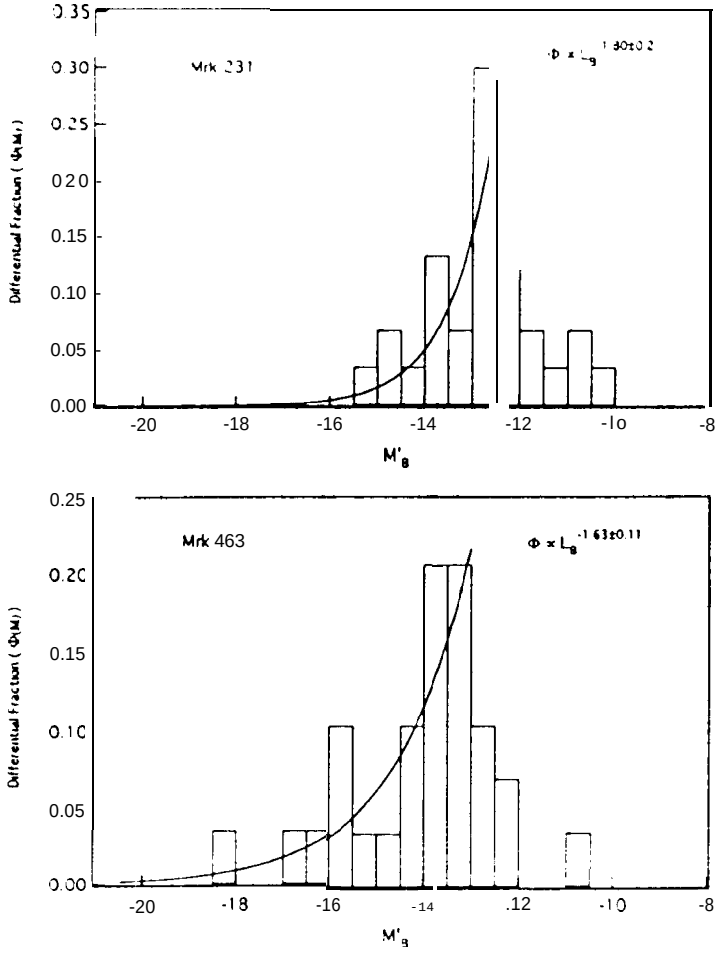

Fig. 9.—

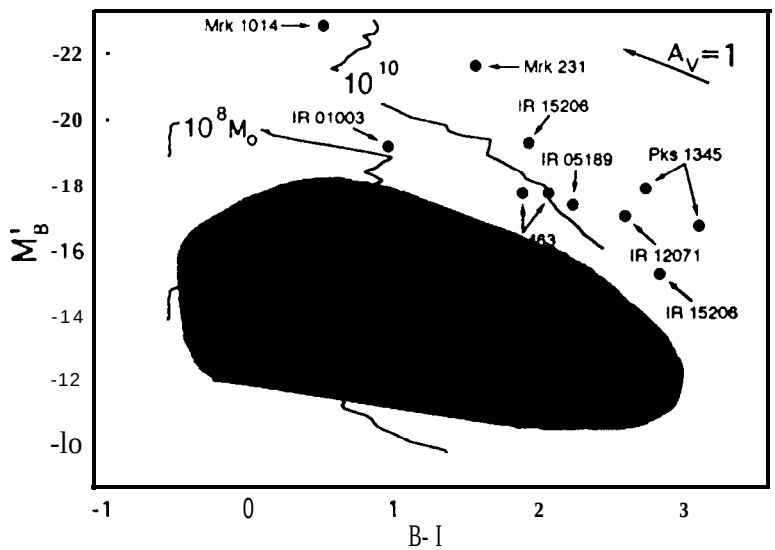
Mrk 1014
10^{10}
Mrk 231
A_V=1
IR 15206
IR 01003
$10^8 M_o$
IR 05189
Pks 1345
IR 12071
IR 15206
M'_B
-22
-20
-18
-16
-14
-12
-lo
-1
0
1
2
3
B-I

Fig. 11. -

TABLE 1

WARM ULIGs OBSERVED BY HST

Name	RA (J2000.0)	Dec	z	$\log \frac{L_{IR}}{L_\odot}$	$\log \frac{L_{bol}}{L_\odot}$	F439W (See)	F814W (see)
IRAS 01003-2238	01:02:49.83	−22:21:56.3	0.118	12.22	12.28	3030	1100
Mrk 1014	01:59:50.18	00:23:41.5	0.163	12.50	12.80	1380	480
IRAS 05189–2524	05:21:01.53	−25:21:46.7	0.042	12.08	12.17	2830	1313
IRAS 08572+3915	09:00:25.42	39:03:54.2	0.058	12.10	12.19	2830	1320
IRAS 12071–0444	12:09:45.10	−05:01:13.7	0.129	12.32	12.38	2500	1200
Mrk 231	12:56:14.24	56:52:26.1	0.042	12.52	12.67	2226	712
Pks 1345+12	13:47:33.55	12:17:24.5	0.122	12.25	12.41	2700	985
Mrk 463	13:56:02.74	18:22:18.3	0.051	11.77	12.03	1030	360
IRAS 15206+3342	15:22:37.96	33:31:36.6	0.125	12.16	12.24	3000	1030

NOTE.—names as given in Sanders et al. (1988 b), with new astrometric positions derived from the STScI Digital Sky Survey.

NOTE.—redshift and L_{IR} from Kim & Sanders (1996), with additional luminosity needed to compute L_{bol} taken from Sanders e! *al.*(1988b)

TABLE 2

WARM GALAXY KNOTS

Number	Δ RA (")	Δ Dec (")	m_B (mag)	m_I (mag)	R_{eff} " (pc)	Mass ($M_\odot$)
			IRAS 01003-2238			
1	0.74	-0.05	24.25	23.43	65	2E+07
2	0.41	0.00	23..50	23.16	106	2E+06
3	0.28	0.23	23.27	22.78	161	2E+06
4	0.00	0.32	23.82	23.77	.55	1E+06
5†	0.00	0.00	19.27	18.3?	28	3E+08
			Mrk 101. I			
1	2.04	5.54	23.79	23.07	70	3E+06
2	6.91	7.34	23.90	23.29	'90	3E+06
3	-0.22	-0.81	22.47	21.50	1.50	4E+08
4†	o	0	16.40	15.90	<15	3E+09
			IRAS 05189-2524			
1	5.93	-3.08	23.04	21.92	12	2E+07
2	2.02	7.68	<24.68	23.13	64	. . .
3"	-0.09	0.14	18.78	16.55	25	2E+1o
4"	0.09	-0.09	19.01	17.37	27	1E+09
			IRAS 08572+3915			
1	13.55	-3.33	26.00	24.50	74	4E+06
2	11.98	-6.27	24.14	23.38	48	5E+06
3	10.83	-6.55	24.57	24.10	49	2E+05
4	5.91	-7.93	24.58	24.35	67	2E+05
5	4.76	-6.95	23.52	22.98	65	4E+05
6	-3.80	0.76	24.92	24.23	55	1E+05
7	.5.36	2.28	24.08	24.08	140	2E+05
8	0.62	-0.48	23.85	21.58	26	3E+08
9	0.13	-0.25	24.59	22.28	75	2E+08
10	-0.33	-0.16	23.43	22.75	55	5E+05
11†	0.00	0.00	22.90	20.59	114	1E+09
12	-0.02	0.47	24.68	22.42	102	1E+08
13	0.05	0.65	24.79	22.66	71	9E+07
14	0.41	0.57	24.44	23.07	40	1 E+o7
15†	2.88	-4.66	20.54	19.26		...
			IRAS 12071-0444			
1	10.45	-11.44	<27.50	23..53	142	...
2	7.38	-7.96	27.41	24.04	82	2E+09
3	-1.69	-3.6-1	23.55	22.78	54	5E+07
4	-1.60	-8.79	<27.50	22.32	104	...
5	-6.81	-8.28	24.70	24.06	17	8E+05
6	-10.-14	-8.00	25.19	23.74	120	4E+07
7	-6.49	7.73	25.71	23.24	1.50	6E+08
8	0.09	-0.92	22.75	20.52	202	4E+09
9†	0.00	0.00	21.59	19.00	244	4E+10
10	-0.09	0.32	21.61	20.19	112	1E+09
11	-0.37	0.14	22.02	20.40	126	8E+08
12	-0.69	0.00	22.66	21..59	181	2E+08
13	-0.92	-0.23	23.5.5	22.33	112	1E+08
			Mrk 231			
1	1.10	1.68	22.23	21.12	66	3E+07
2	-1.52	-0.90	23.27	20.86	< .20	5E+08
3	1.10	-0.16	22.38	20.86	62	5E+07

TABLE 2—*Continued*

Number	Δ RA (″)	Δ Dec (″)	m_B (mag)	m_I (mag)	R_{eff} [a] (pc)	Mass ($M_\odot$)
22	0.59	-1.32	23.17	23.21	38	3E+05
23	0.36	-1.41	23.53	21.11	2[b]	2E+05
24	-0.29	1.19	22.81	22.34	62	6E+05
25	-0.65	1.39	22.67	21.93	65	1E+07
26	-1.44	0.93	24.00	23.00	81	8E+06
27	-1.15	-1.37	22.95	23.08	62	4E+05
28	-0.56	-0.68	21.50	21.41	100	1E+06
29	-0.93	-0.77	20.88	20.92	109	3E+06
30	-0.79	-0.72	20.86	20.82	77	3E+06
			IRAS 15206+3342			
1	0.69	0.46	21.77	21.96	206	7E+06
2	0.64	-0.14	23.00	20.37	73	3E+09
3	0.83	-0.55	22.30	20.94	159	4E+08
4	0.51	-0,41	22.08	20.18	76	2E+09
5	0.37	-0.74	22.60	21.23	107	3E+08
6†	0.00	0.00	19.29	17.37	57	3E+10
7	-0.05	-0.41	19.50	18.68	104	2E+09
8	-0.14	-0.64	21.54	21.78	84	8E+06
9	-0.51	-0.64	19.45	18.54	88	3E+09
10	-0.74	-0.64	20.43	20.17	67	3E+07
11†	-1.29	-0.32	22.87	20.10	93	2E+10
12	-2.02	-0.74	22.66	20.83	233	1E+09
13	-2.25	-0.83	22.64	20.81	221	1E+09
14	-0.83	0.46	23.33	21.79	152	2E+08
15	-1.01	0.23	23.28	22.07	90	1E+08
16	-1.20	0.23	22.37	21.75	101	7E+06
17	-1.52	0.09	22.44	20.46	108	2E+09
18	-1.93	0.05	23.73	21.91	87	3E+08
19	-2.76	-0.09	21.74	20.55	233	6E+08

NOTE.—† putative active nucleus - identified on the basis of B-I color, size, and absolute B magnitude (in all cases the brightest object at B).

NOTE.—″ the two listed nuclei appear to actually be a single nucleus split by a dust lane.

NOTE.—[a] effective radius defined by half-width half-intensity.